



TITLE:

# A Monolithic Dual-Color Total-Internal-Reflection-Based Chip for Highly Sensitive and High-Resolution Dual-Fluorescence Imaging

AUTHOR(S):

Le, Nam Cao Hoai; Dao, Dzung Viet; Yokokawa, Ryuji; Wells, John C.; Sugiyama, Susumu

---

CITATION:

Le, Nam Cao Hoai ...[et al]. A Monolithic Dual-Color Total-Internal-Reflection-Based Chip for Highly Sensitive and High-Resolution Dual-Fluorescence Imaging. JOURNAL OF MICROELECTROMECHANICAL SYSTEMS 2009, 18(6): 1371-1381

ISSUE DATE:

2009-12

URL:

<http://hdl.handle.net/2433/109814>

RIGHT:

© 2009 IEEE. Personal use of this material is permitted. However, permission to reprint/republish this material for advertising or promotional purposes or for creating new collective works for resale or redistribution to servers or lists, or to reuse any copyrighted component of this work in other works must be obtained from the IEEE.

# A Monolithic Dual-Color Total-Internal-Reflection-Based Chip for Highly Sensitive and High-Resolution Dual-Fluorescence Imaging

Nam Cao Hoai Le, Dzung Viet Dao, Ryuji Yokokawa, *Member, IEEE*,  
John C. Wells, and Susumu Sugiyama, *Member, IEEE*

**Abstract**—We report a dual-color total-internal-reflection (TIR)-based chip that can generate two overlapping evanescent fields with different wavelengths for simultaneous imaging of two types of fluorophores. We derived a general relationship among the dimensions of the components of the chip to guarantee the overlap of two evanescent fields. Optical simulation results also confirm the generation and overlap of two evanescent fields. Using Si bulk micromachining and poly(dimethylsiloxane) (PDMS) casting, our fabrication method integrates all miniaturized optical components into one monolithic PDMS chip. Thus, assembly is unnecessary, and misalignment is avoided. Our PDMS chip can be employed with various sample delivery platforms, such as glass slide, flow cell, microchannel, etc. We first demonstrated the capability of the chip by imaging TIR fluorescent spots of a mixture of two fluorophores, namely, fluorescein and tetramethylrhodamine. We then employed the chip to observe the Brownian motion of a mixture of Nile-red and dragon-green 500-nm microbeads. Our chip could potentially be integrated into a micro-total analysis system for highly sensitive and high-resolution dual-fluorescence imaging applications. [2009-0188]

**Index Terms**—Dual-color total-internal-reflection fluorescent microscopy (TIRFM), dual-fluorescence imaging, evanescent

Manuscript received March 25, 2009. First published October 13, 2009; current version published December 1, 2009. This work was supported in part by the Kyoto Nanotech Cluster and in part by Research for Promoting Technological Seeds Grant 09-043 and by PRESTO/CREST from the Japan Science and Technology Agency (JST). The work of N. C. H. Le was supported by a doctoral scholarship from the Ministry of Education, Culture, Sports, Science and Technology, Japan. An earlier version of this paper was presented at IEEE Sensors 2008, Lecce, Italy, October 26–29. Subject Editor S. Merlo.

N. C. H. Le was with the Graduate School of Science and Engineering, Ritsumeikan University, Shiga 525-8577, Japan. He is now with the Biomedical Diagnostics Institute, Dublin City University, Dublin, Ireland (e-mail: nam.caohai@dcu.ie).

D. V. Dao is with the Research Organization of Science and Engineering, Ritsumeikan University, Shiga 525-8577, Japan (e-mail: dzung@fc.ritsumei.ac.jp).

R. Yokokawa is with the Department of Microengineering, Kyoto University, Kyoto 606-8501, Japan, and also with Core Research of Evolutional Science and Technology (CREST)/Precursory Research for Embryonic Science and Technology (PRESTO), Saitama 332-0012, Japan (e-mail: ryuji@me.kyoto-u.ac.jp).

J. C. Wells is with the Department of Civil and Environmental Engineering, Ritsumeikan University, Shiga 525-8577, Japan (e-mail: jwells@se.ritsumei.ac.jp).

S. Sugiyama is with the Ritsumeikan Global Innovation Research Organization, Ritsumeikan University, Shiga 525-8577, Japan (e-mail: sugiyama@fc.ritsumei.ac.jp).

Color versions of one or more of the figures in this paper are available online at <http://ieeexplore.ieee.org>.

Digital Object Identifier 10.1109/JMEMS.2009.2030938

fields, micro-total analysis systems ( $\mu$ -TAS), poly(dimethylsiloxane) (PDMS).

## I. INTRODUCTION

AMONG MANY fluorescence-based investigation techniques, such as epi-fluorescence microscopy, confocal fluorescence microscopy, fluorescence correlation spectroscopy, etc., total-internal-reflection fluorescence microscopy (TIRFM) has received increasing recognition in the past decades due to its unique capabilities. The working principle of TIRFM relies on the evanescent-field illumination generated by TIR at a liquid/dielectric interface [1]. This evanescent field, whose depth of penetration is on the order of 100–300 nm, is capable of selectively exciting fluorophores in the liquid region very close to the dielectric material. The extremely thin excitation depth greatly reduces the background noise, which is often the biggest problem in fluorescence detection and imaging, since the fluorophores in the bulk liquid are not excited. Fluorescent images obtained by this evanescent excitation typically possess very high signal-to-noise ratio and virtually no out-of-focus signal from the bulk liquid.

Within the last two decades, TIRFM has been increasingly applied by many researchers for studying the dynamics of biological systems from cell membranes to single biomolecules [2]–[8] and for characterizing micro-/nanofluidic flows [9]–[13]. Very recently, some groups have proposed several configurations of dual-color TIRFM that can generate two overlapping evanescent fields with different excitation wavelengths for simultaneous detection of two different fluorophores either inside a cell or on a glass surface. In cell imaging, Tengholm *et al.* [14] reported a prism-type dual-color TIRFM system for the simultaneous detection of recruitment and dissociation of two differently labeled fluorescent proteins to and from the plasma membrane. Schmoranz and Simon [15] used an objective-type dual-color TIRFM system to observe the transport, docking, and fusion of vesicles along microtubule cytoskeletons in a cell membrane. Similarly, Ikuko *et al.* [16] utilized an objective-type dual-color TIRFM system to study the colocalization of two single molecules in living cells. For application on a glass surface, using a prism-type dual-color TIRFM, Kang *et al.* [17] and Lee *et al.* [18] reported the detection of the hybridization and interaction of two single biomolecules on

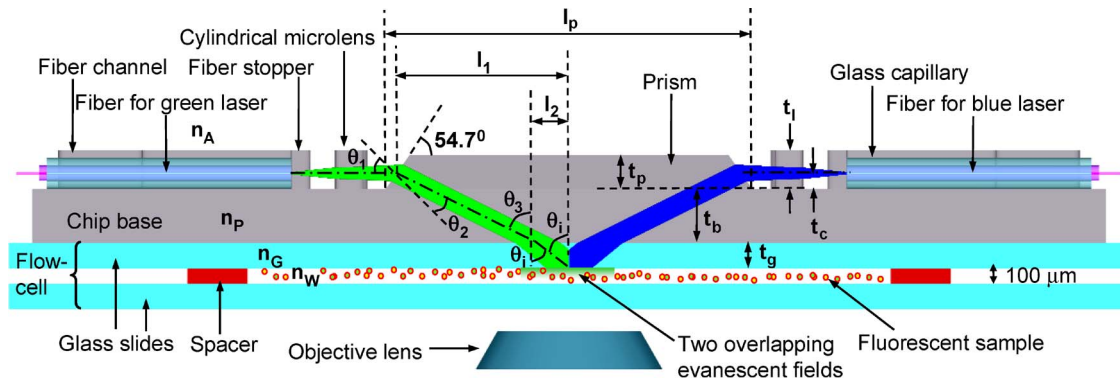


Fig. 1. Cross-sectional view (not to scale) of the dual-color TIR-based chip with glass flow cell. The nomenclature of the chip dimensions are listed in Table I. The incident angles of green and blue excitations are  $68.1^\circ$  and  $70.0^\circ$ , respectively. They are both larger than the critical angle  $\theta_C = 61^\circ$  (for the glass/water interface), satisfying the condition for TIR for both excitation lasers. The overlapping evanescent fields simultaneously excite the mixture of two different fluorophores. The emission is passed to an objective lens, chromatically separated by a specialized filter setup and imaged side by side on a CCD camera.

the surface of a glass chip. Leutenegger *et al.* [19] combined an objective-type dual-color TIRFM system with a cross-correlation spectroscopy to study the binding of two dual-labeled double-stranded DNA molecules on glass surfaces.

Although those conventional objective- and prism-type dual-color TIRFM systems have been powerful tools in the aforementioned fields, they are highly costly, bulky, and elaborate and time consuming in assembly and alignment. Miniaturized and integrated dual-color TIR-based devices might offer lower cost and easier setup than conventional dual-color TIRFM systems. Furthermore, such devices might allow integration with micro-total analysis systems ( $\mu$ -TAS) for highly sensitive dual-fluorescence detection and imaging applications. Recently, some groups, including ours, have proposed various configurations of integrated, miniaturized, and low-cost TIR-based devices [20]–[25]. However, these devices can only provide one excitation wavelength for the detection of one type of fluorophores.

We propose here, to our knowledge, the first integrated and miniaturized dual-color TIR-based device fabricated using Si micromachining and poly(dimethylsiloxane) (PDMS) casting technology. This paper presents the design, analysis, simulation, fabrication, and evaluation of the proposed chip. We derived a set of equations governing the overlap condition of two evanescent fields in a given chip configuration. A simple yet effective fabrication method has enabled us to integrate all miniaturized optical components including a prism, cylindrical microlenses, and fiber alignment channels into one monolithic PDMS chip. Demonstrations of the chip for the simultaneous imaging of mixtures of two fluorescent dyes and two different fluorescent microbeads will be presented.

## II. DESIGN, ANALYSIS, AND SIMULATION

### A. Design Concept

The cross section of the chip with the optical path is schematically shown in Fig. 1, while the nomenclature of the chip dimensions is listed in Table I. The monolithic PDMS chip consists of a prism in the center, two cylindrical microlenses, two fiber alignment channels, and a common base underneath. The  $54.7^\circ$ -inclined surfaces of the prism are (111) crystal planes

TABLE I  
NOMENCLATURE OF THE PRINCIPAL PARAMETERS OF THE DEVICE

Symbol	Quantity
$l_p$	Length of base of prism
$w_p$	Width of base of prism
$l_b$	Length of chip base
$w_b$	Width of chip base
$t_b$	Thickness of chip base
$t_g$	Glass slide thickness
$t_p$	Height of prism
$t_c$	Height of core center of optical fiber
$t_l$	Height of cylindrical lens and fiber alignment channel
$r_1$	Rear radius of curvature of cylindrical microlens
$r_2$	Front radius of curvature of cylindrical microlens
$f$	Rear focal length of cylindrical microlens
$u_l$	Thickness of cylindrical microlens
$w_l$	Effective width of cylindrical microlens
$c_1$	Rear opening length of fiber alignment channel
$c_2$	Contact length of fiber alignment channel
$c_3$	Front opening length of fiber alignment channel
$c_{dr}$	Rear opening gap of fiber alignment channel
$c_c$	Contact gap of fiber alignment channel
$c_{df}$	Front opening gap of fiber alignment channel
$c_t$	Gap of throat of fiber alignment channel
$c_e$	Gap of exit of fiber alignment channel

defined by the standard TMAH wet etching of a (100) single-crystal Si wafer. A glass flow cell, reversibly bonded to the chip base by the van der Waals contact between PDMS and glass, serves as a sample delivery platform. Although relatively weak, this bond itself is sufficient to prevent any TIR occurring at the PDMS/air/glass interface [26]. The flow cell, which has 24-mm-length, 7–8-mm-width, and 100- $\mu$ m-height dimensions, is prepared using two spacers (paper slips, 2 mm  $\times$  25 mm in size and 100  $\mu$ m in thickness) coated with grease (Apiezon M grease, M&I Materials Ltd., U.K.) between two cover glasses (24 mm  $\times$  36 mm in size and 0.12–0.17 mm in thickness, Matsunami Co., Japan) [24]. Two single-mode optical fibers (core/cladding = 9.2  $\mu$ m/125  $\mu$ m and numerical aperture ( $NA$ ) = 0.12, Sumitomo Inc., Japan) are concentrically inserted and glued with epoxy in two glass capillaries ( $I.D./O.D.$  = 128  $\mu$ m/250  $\mu$ m, NEG Co., Ltd., Japan). These two glass capillaries are then aligned and stopped by the fiber alignment channels on both sides of the device (Fig. 2). The gradual contraction of the rear of the fiber alignment channels

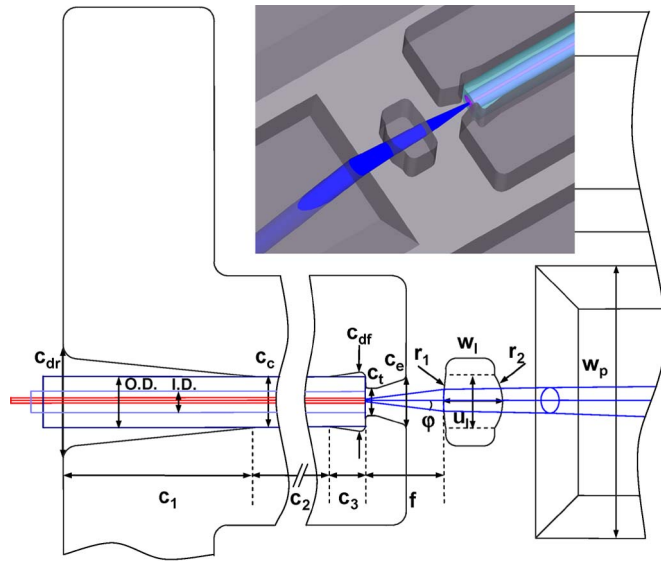


Fig. 2. Partial top view (not to scale) of the fiber alignment channel, the cylindrical microlens, and the prism on one side of the chip. The inset shows the 3-D model of the structure when the glass capillary containing the fiber was inserted. The nomenclature of the dimensions is listed in Table I.

( $c_{dr} = 400 \mu\text{m}$ ,  $c_c = 240 \mu\text{m}$ , and  $c_1 = 2444 \mu\text{m}$ ) facilitates the insertion of the glass capillaries. Once inside the channels, the glass capillaries are clamped by the flexible PDMS walls ( $c_2 = 2160 \mu\text{m}$ ) with  $240\text{-}\mu\text{m}$  contact gap. At the end of the fiber alignment channels, the capillaries are stopped by nozzle-like stoppers ( $c_3 = 278 \mu\text{m}$ ,  $c_{df} = 312 \mu\text{m}$ ,  $c_t = 120 \mu\text{m}$ , and  $c_e = 520 \mu\text{m}$ ). The dimensions of the stoppers are chosen so that not only the fibers are stopped ( $c_t = 120 \mu\text{m}$  is smaller than  $O.D. = 250 \mu\text{m}$  of capillary) at a rear focal distance  $f$  from the cylindrical microlens but also allow the light beam to emit freely from the fibers without interference with any part of the fiber alignment channels (Fig. 2).

The green laser (543 nm) emitting from the left fiber is collimated by the left microlens, refracted twice at the air/PDMS and PDMS/glass interfaces, respectively, and finally generates a green evanescent field at the glass/water interface [24]. In a similar manner, the blue laser (473 nm) from the right optical fiber will also generate another blue evanescent field at the same glass/water interface. In our dual-color TIRFM chip, it is essential to ensure the overlap of the centers of the two evanescent fields generated by the two excitation beams, so that two types of fluorophores in the same field of view can be simultaneously excited by their respective excitation wavelengths. Fluorescent emission from the fluorescent sample is passed to the objective lens of an inverted microscope equipped with a specialized filter system and imaged onto a charge-coupled-device (CCD) camera. In the following sections, we will combine optical analysis and simulation to find the values of the remaining design parameters listed in Table I to guarantee the overlap of the two evanescent fields. The dimensions of the cylindrical microlens will also be found with the aid of ray-tracing software and confirmed with ray analysis.

According to our design concept, the chip can be reversibly bonded to various sample delivery platforms, such as PDMS microchannels, glass microchannels, glass slides, or glass flow

cells. This feature is very useful since the chip can be reused, while the sample delivery platforms can be disposable. It also facilitates surface treatments or immobilizations on the sample delivery platforms before observations. Furthermore, by simply turning the device upside down, it is possible to use it with both upright and inverted fluorescent microscopes [25].

## B. Optical Ray Analysis

For simplicity, optical analysis only considered the central ray of the beam. We assumed that the bottom surface of the glass capillary touches the base, so the central ray of the beam will be at a height  $t_c$  from the chip base. Since the chip is symmetric, optical ray analysis from the green excitation side was performed first. Using Snell's law and geometric relationships from Fig. 1, the following equations could easily be derived:

$$\theta_1 = 90^\circ - 54.7^\circ = 35.3^\circ \quad (1)$$

$$\theta_2 = \sin^{-1} \left( \frac{n_A}{n_P} \sin \theta_1 \right) \quad (2)$$

$$\theta_3 = 90^\circ - \theta_1 + \theta_2 = 90^\circ - \theta_1 + \sin^{-1} \left( \frac{n_A}{n_P} \sin \theta_1 \right) \quad (3)$$

$$\theta_i = \sin^{-1} \left( \frac{n_P}{n_G} \sin \theta_3 \right) \quad (4)$$

$$\theta_i = \sin^{-1} \left[ \frac{n_P}{n_G} \sin \left( 90^\circ - \theta_1 + \sin^{-1} \left( \frac{n_A}{n_P} \sin \theta_1 \right) \right) \right] \quad (5)$$

where  $n_A$ ,  $n_P$ , and  $n_G$  are the refractive indices of air, PDMS, and glass, respectively. It should be noted that the refractive index of PDMS depends on wavelength, mixing ratio, and curing temperature [27]. As an approximation, we employed Conrady's formula with three index-wavelength pairs (i.e., 1.465 at 460 nm, 1.422 at 610 nm [27], and 1.43 at 580 nm [28]) of PDMS to obtain a continuous fit [29]. The refractive indices of PDMS at 543 and 473 nm were then estimated to be 1.44 and 1.46, respectively. The refractive index of the cover glass is specified by the manufacturer (Matsunami Co., Japan) to be 1.52 and is negligibly dependent on wavelength. For green excitation (543 nm), substituting  $n_P = 1.44$ ,  $n_G = 1.52$ ,  $n_A = 1$ , and  $\theta_1 = 35.3^\circ$  into (5), we have  $\theta_i = 68.1^\circ$ . The same equation (5) can also be used if we consider the other side of the chip, i.e., blue excitation (473 nm), where  $n_P = 1.46$ ,  $n_G = 1.52$ ,  $n_A = 1$ , and  $\theta_1 = 35.3^\circ$ , resulting in  $\theta_i = 70.0^\circ$ . Clearly, the incident angles of both excitation wavelengths are greater than the critical angle of  $\theta_c = 61^\circ$  (for the glass/water interface), so the condition for TIR is satisfied for both excitation lasers [24].

As mentioned earlier, we must ensure the overlap of the centers of two evanescent fields. From Fig. 1, it can be observed that this condition will be met if the centers of the green and blue evanescent fields both fall on the center of the prism projected on the cover glass of the flow cell. Considering again the green-excitation side of the chip, this condition can be expressed by

$$l_1 = \frac{l_p}{2} - \frac{t_c}{\tan 54.7^\circ}. \quad (6)$$



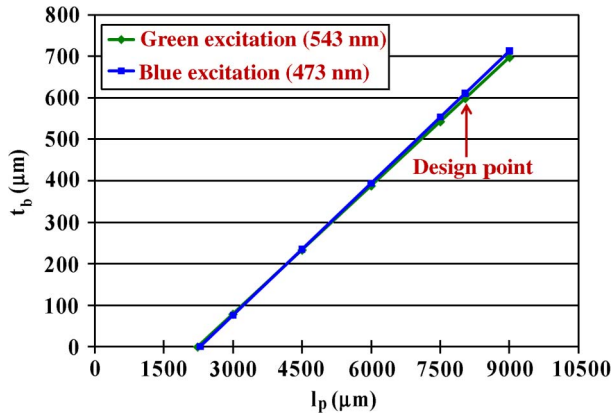


Fig. 3. Linear relationship obtained by ray analysis of chip base thickness  $t_b$  and chip prism size  $l_p$  for two excitation wavelengths to guarantee the overlap of the centers of two evanescent fields, as expressed in (6).

Again from Fig. 1, (7) and (8) can be derived as

$$l_2 = t_g \tan \theta_i \quad (7)$$

$$t_b + t_c = \frac{l_1 - l_2}{\tan \theta_3}. \quad (8)$$

Substituting (7) into (8), and then  $l_1$  from (8) into (6), we have

$$t_b = \frac{l_p}{2 \tan \theta_3} - \frac{t_g \tan \theta_i}{\tan \theta_3} - t_c \left( \frac{1}{\tan \theta_3 \tan 54.7^\circ} + 1 \right). \quad (9)$$

The cover glasses have a nominal thickness  $t_g$  of 170  $\mu\text{m}$ . The O.D. of the glass capillaries is 250  $\mu\text{m}$ , yielding a  $t_c$  of 125  $\mu\text{m}$ . This value of  $t_c$  is obviously smaller than both prism height  $t_p$ , typically in the range of 250–270  $\mu\text{m}$  according to the wet-etching time, and cylindrical-lens height  $t_l$  defined by the 300- $\mu\text{m}$ -thick Si wafers used in fabrication. While  $t_c$  must be smaller than both  $t_l$  and  $t_p$ , it is necessary for the central ray of the beam to hit the prism in the midside node so that the divergent marginal rays, defined by the NA of the fiber, will still be confined within the height of the prism. Finally,  $t_b$  was plotted against varying  $l_p$ 's by putting the relevant parameters into (9) for green and blue excitations (Fig. 3). These lines show a linear relationship between chip base thickness  $t_b$  and chip prism size  $l_p$  in order for the center of the evanescent fields to fall in the center of the prism projected on the flow cell.

The smallest prism base lengths would be 2235 and 2288  $\mu\text{m}$  for green and blue excitations, respectively, for a chip base thickness  $t_b$  of zero, i.e., when the prism and lenses are directly attached to the glass slide. However, a finite chip base thickness  $t_b$  is necessary to support and integrate the components of the chip. Considering the chip size with respect to the glass flow-cell size, the number of chips on a 4-in wafer, and the availability of the sizes of O-ring for the wet anisotropic etching jig, we chose  $l_p = 8042$   $\mu\text{m}$ , yielding  $t_b = 599$  and 611  $\mu\text{m}$  for green and blue excitations, respectively. Choosing  $w_p = 2966$   $\mu\text{m}$  and taking into account the total length and width of the supporting wings of the fiber alignment channel of 5205 and 9966  $\mu\text{m}$ , respectively, the resulting chip size would be 10 mm  $\times$  20 mm  $\times$  0.9 mm in  $L \times W \times T$ . This chip would be sufficiently small to attach wholly to the cover glass of the flow cell (24 mm  $\times$  36 mm in  $L \times W$ ) yet large enough to be handled manually.

### C. Simulation

Other than ray analysis, the ZEMAX EE 2007<sup>1</sup> optical simulation package was also employed to confirm our design concept and to find the dimensions of the cylindrical microlens, as well as the design parameters of the chip. First, the sequential mode was used to solve a three-variable (i.e., focal length, lens thickness, and radius of curvatures) optimization problem with target values of Gaussian beam radius and beam divergence angle to obtain optimal microlens parameters. For simplicity, we used the following assumptions and parameters in the simulation: The beam from the single-mode fiber had a Gaussian intensity distribution; the NA and mode field diameter (MFD) of the fiber were 0.12 and 9.2  $\mu\text{m}$ , respectively, obtained from the manufacturer (Sumitomo Inc., Japan); the excitation wavelength was 543 nm; and the number of analysis rays was 1000. It should be noted that, however, a standard single-mode fiber would typically have a cutoff wavelength near 1300 nm [30]. Thus, at a wavelength of 543 nm (or 473 nm) used in this paper, the single-mode fibers might transmit not only a fundamental mode, which has a Gaussian distribution, but also higher modes, unless a mechanism to filter out these additional modes is introduced [31]. The  $1/e$  beam radius  $r = 30$   $\mu\text{m}$  (at the imaging plane that is 140  $\mu\text{m}$  after the microlens where the prism base is located), together with the beam  $0^\circ$  divergence angle, was chosen as the target value for the optimization problem.

The obtained optimal microlens is of convex-convex type with front radius of curvature  $r_1 = -457$   $\mu\text{m}$ , rear radius of curvature  $r_2 = 1628$   $\mu\text{m}$ , thickness  $u_l = 557$   $\mu\text{m}$ , and rear focal length of  $f = 488$   $\mu\text{m}$  [Figs. 2 and 4(a)]. Fig. 4(b) shows the spot diagram obtained in the imaging plane. Since the cylindrical microlens can only collimate the laser beam in the horizontal direction, the beam diverges in the vertical direction when propagating along the chip. The elliptical shape of the spot diagram has a root-mean-square (rms) radius of 75  $\mu\text{m}$ , which is smallest compared to other lens configurations (data not shown). The widths of the beam obtained by using ZEMAX EE in both horizontal and vertical directions [Fig. 4(b)] agree very well with the ray analysis results obtained by using Snell's law in Fig. 4(c) and (d), respectively. The 243- $\mu\text{m}$  width of the beam in the vertical direction requires the use of a glass capillary to increase the height of the fiber core to 125  $\mu\text{m}$ . Since the prism height  $t_p$  is larger than 250  $\mu\text{m}$ , we can expect that all rays of the beam will enter the prism. We also solved the problem with blue wavelength (473 nm) and found that the lens dimensions differ negligibly from the case of green wavelength (543 nm). Thus, these dimensions were applied for both cylindrical lenses.

In order to confirm the existence and overlap of two evanescent fields, the nonsequential mode in ZEMAX EE was used. We used the same parameters mentioned earlier but with an additional blue laser beam with a wavelength of 473 nm. The cover-glass thickness  $t_g$  and the height of the fiber core  $t_c$  were also fixed at 170 and 125  $\mu\text{m}$ , respectively. A detector surface, whose size is equal to the base of the prism, was inserted between the interface of glass and water to collect the incoherent irradiance of green and blue excitations. In previous work, the

<sup>1</sup> ZEMAX Corporation. [Online]. Available: www.zemax.com.

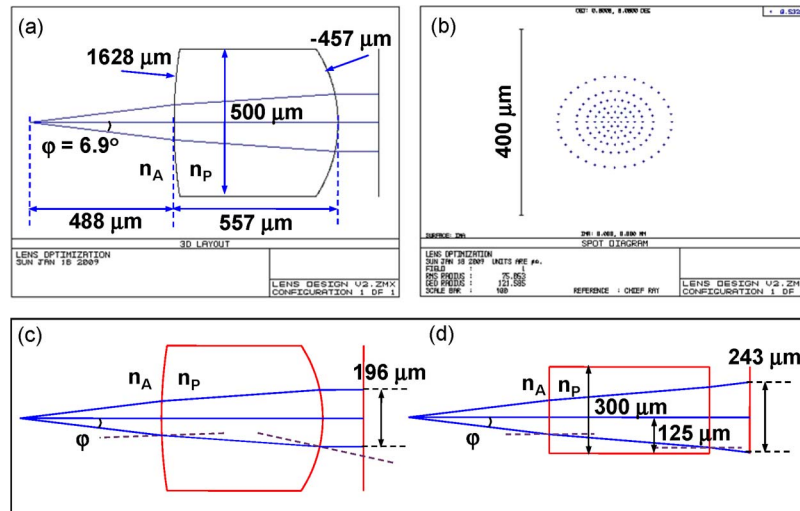


Fig. 4. (a) Optimal lens dimensions obtained using ZEMAX EE simulation and (b) spot diagram on the imaging plane at  $140\ \mu\text{m}$  after the lens. (c) and (d) Widths of the spot diagram in the horizontal and vertical directions, respectively, obtained using ray analysis agree very well with the simulation result in (b).

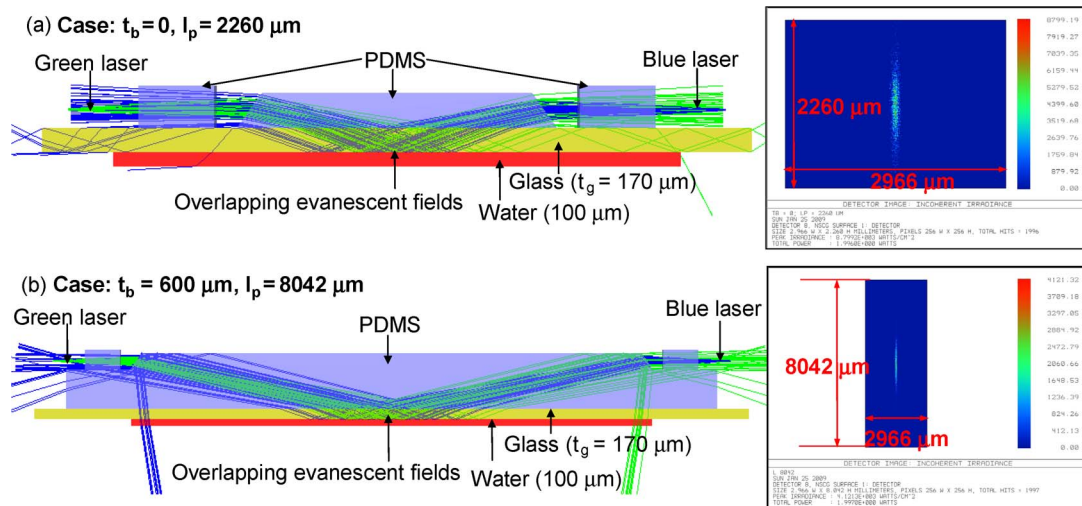


Fig. 5. Dual-beam ray-tracing results and incoherent irradiances detected on the glass/water interface, showing that two evanescent fields have been generated and overlapped in the center of the prism projected on the flow cell for two cases: (a) when chip base thickness  $t_b = 0$  and (b) when prism length  $l_p = 8042\ \mu\text{m}$ , leading to  $t_b = 600\ \mu\text{m}$ , which is also the design case.

incoherent irradiance spots at the glass/water interface were used to estimate the size and shape of the evanescent fields [24]. In this work, we could control the overlap of two evanescent fields by finding the  $t_b$  for which the centers of two incoherent irradiance spots fall on the center of the prism while varying the prism length  $l_p$ . Fig. 5(a) shows the extreme case when the chip base thickness  $t_b$  is zero, i.e., when glass directly is attached to the prism and the lenses, while Fig. 5(b) shows the design case when prism length  $l_p$  is  $8042\ \mu\text{m}$ , leading to a  $t_b$  of  $600\ \mu\text{m}$ . In both cases, the two incoherent irradiance spots overlap at the center of the prism projected onto the glass flow cell. The size of the evanescent field in the design case is estimated to be  $2500\ \mu\text{m}$  in length and  $190\ \mu\text{m}$  in width [Fig. 5(b)]. The simulation results of  $t_b$  versus  $l_p$  are shown in Fig. 6, agreeing very well with the analysis results in Fig. 3. The small discrepancy might be attributed to the center ray versus whole beam tracing of optical ray analysis and simulation, respectively, and the capability of ZEMAX EE to take into account the index–wavelength dependence automatically in the

simulation. Since the evanescent fields are quite long, a small difference in  $t_b$  for green and blue excitations would have negligible effect on their overlap. In fabrication,  $t_b$  is controlled by the volume of PDMS during casting.

### III. FABRICATION PROCESS

The polymer chip was fabricated using the standard Si bulk micromachining and PDMS casting techniques adapted from previous work [24]. The process flow is shown in Fig. 7(a)–(g). First, a  $1.3\text{-}\mu\text{m}$ -thick oxide layer was formed on both sides of a  $300\text{-}\mu\text{m}$  (100) single-crystal Si wafer by pyrogenic oxidation [Fig. 7(a)]. In the second step, the prism patterns on the front side and the microlens and the fiber channel patterns on the back side were defined by photolithography and  $\text{SiO}_2$  etching by buffered HF (BHF) solution [Fig. 7(b)]. The wafer was then diced into single chips ( $27\ \text{mm} \times 27\ \text{mm}$ ) for the next steps. The third step was TMAH anisotropic wet etching [Fig. 7(c)] on the opened window of the prism on the front side. A Teflon jig was

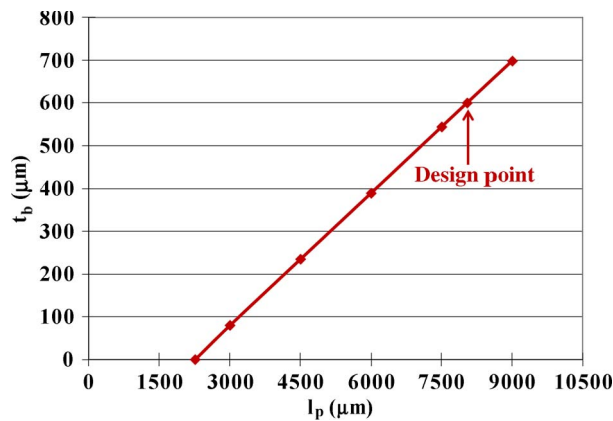


Fig. 6. Linear relationship obtained by using ZEMAX EE simulation of chip base thickness  $t_b$  and chip prism size  $l_p$  for two excitation wavelengths to guarantee the overlap of the centers of two evanescent fields. This result agrees very well with the ray analysis result in Fig. 3.

used to protect the back side, containing opened Si patterns for the microlens and the fiber alignment channel during TMAH etching. A TMAH etch for 6 h was sufficient to etch up to 270- $\mu\text{m}$  depth for an approximate etching rate of 0.75  $\mu\text{m}/\text{min}$ .

The fourth step was through-wafer deep reactive-ion etching (DRIE) on the back side to create the cavities for the microlens and the fiber alignment channels [Fig. 7(d)]. It has been reported that a through-wafer DRIE process gives a very complex roughness topography at different depths on the sidewalls [32]–[34]. We have employed a thick  $\text{SiO}_2$  mask with a constant trench width of 50  $\mu\text{m}$  to ensure smooth and straight sidewalls in through-wafer Si etching by DRIE [33]. With an optimized DRIE process, we could etch through 300- $\mu\text{m}$ -thick Si chips within 90 min, yielding relatively smooth and vertical sidewalls. Both roughness average ( $R_a$ ) and rms roughness were below 50 nm. The chips were then cleaned in Piranha for 30 min, and the remaining  $\text{SiO}_2$  was completely removed by BHF etching. We further reduced the roughness of the Si molds by three cycles of oxidation (the  $\text{SiO}_2$  thicknesses were 370, 230, and 230 nm, respectively) and BHF etching [Fig. 7(e)] [35]. The  $\text{SiO}_2$  growth has been shown to depend greatly on the feature geometry, meaning that convex corners grow faster than concave corners [36]. Accordingly, the sharp and high roughness features will be more oxidized and will be removed faster during BHF etching. With this process, we could achieve the  $R_a$  and rms roughness of the Si molds below 25 nm. This order of roughness, when transferred to PDMS, would be sufficiently small to fulfill Marechal's criterion for scattering for both excitation wavelengths [37]. Fig. 8(a) and (b) shows a photograph and the scanning-electron-microscope (SEM) micrographs of the Si mold, respectively.

Next, in the sixth step, the Si mold was sealed to a PDMS film (thickness of 160  $\mu\text{m}$ ) stretching on top of a glass substrate to form a close mold [Fig. 7(f)]. The mold was then placed onto a flat hot plate. A PDMS (Silpot184W/C, Dow Corning, Japan) mixture (1:10 curing agent: prepolymer) was poured on the mold and was allowed to self-planarize for 1 h. Curing on the hot plate was done at 90  $^\circ\text{C}$  for 30 min. Finally, the PDMS chip replica was carefully removed from the Si mold [Fig. 7(g)]. As mentioned in Section II-A, the chip base thickness  $t_b$  was con-

trolled by the volume of liquid PDMS mixture during casting. For a Si mold of 27 mm  $\times$  27 mm, the volume of liquid PDMS required was 0.3 mL to achieve a  $t_b$  of approximately 600  $\mu\text{m}$  (Fig. 9). Using a single Si mold, the dual-color TIR-based chips can be replicated by repeated PDMS castings. Fig. 8(c) and (d) shows a photograph and the SEM micrographs of the PDMS chip, respectively.

#### IV. EXPERIMENTAL SETUP AND MATERIALS

Fig. 10(a) shows the experimental setup using the dual-color TIR-based chip. A blue laser (DPBL-9050, Photop Suwtech, China, maximum power of 50 mW, 473 nm) and a green laser (05-LGR-173, Melles Griot, Inc., U.S., maximum power of 2 mW, 543 nm) were coupled into two single-mode optical fibers (core/cladding = 9.2  $\mu\text{m}/125 \mu\text{m}$  and  $NA = 0.12$ , Sumitomo Inc., Japan). The chip was placed so that the glass flow cell facing an objective lens (10 $\times$  or 60 $\times$ , Olympus Inc., Japan) of an inverted microscope (IX71, Olympus Inc., Japan) equipped with an electron-multiplier CCD (EMCCD) camera (iXon EM+ DU-897, Andor Technology plc., Northern Ireland). A Dual-View (Optical Insights Inc., U.S.) was inserted between the emission port of the microscope and the C-mount of the camera to split the emission with a wavelength that was larger than 560 nm [mostly from tetramethylrhodamine (TMR) and Nile red (NR)] to the emission filter ET 585/40 against the emission with wavelength smaller than 560 nm [mostly from fluorescein (FI) and dragon-green (DG)] to the emission filter ET 515/30 [Fig. 10(b)].

A mixture of TMR (C-1171, Ex/Em = 532 nm/556 nm, Molecular Probes Inc., U.S.) and FI (CI 45350, Ex/Em = 494 nm/521 nm, Wako, Japan) in DMSO at concentrations of 0.3 and 3.3 mM, respectively, were used in the observation of evanescent-field fluorescent spots, i.e., TIR fluorescent spots. A mixture of suspensions of carboxyl fluorescent NR beads (CFP-0556-2, Ex/Em = 532 nm/556 nm, 400–600 nm in diameter, SpheroTech, Inc., U.S.) and DG beads (CP01F/8206, Ex/Em = 480 nm/520 nm, 510 nm in diameter, Bangs Laboratories, Inc., U.S.) dispersed in Tween20/DI water solution (0.05%), both at 0.05%  $w/v$  concentration, was used for the observation of the Brownian motion. The chip setup was fixed on the stage of the microscope, as shown in Fig. 10(c). In each experiment, a fluorescent sample with a volume of 10  $\mu\text{L}$  was injected into the flow cell. For all experiments, the power of the lasers from both fibers were set to 0.52 mW measured by a laser power meter (PM-221, Neoark Corp., Japan). Fluorescent images were acquired and analyzed by image processing software (Andor IQ, Andor Technology plc., Northern Ireland). All experiments were performed in a dark room.

#### V. RESULTS AND DISCUSSION

##### A. Imaging of Overlapping TIR Fluorescent Spots From Two Fluorescent Dyes

Fig. 11(a)–(c) shows the fluorescent images of TIR fluorescent spots on the glass flow cell deposited with a mixture of TMR and FI dyes on the ET 585/40 and ET 515/30 emission channels. Although the fluorescent dye solutions were spread



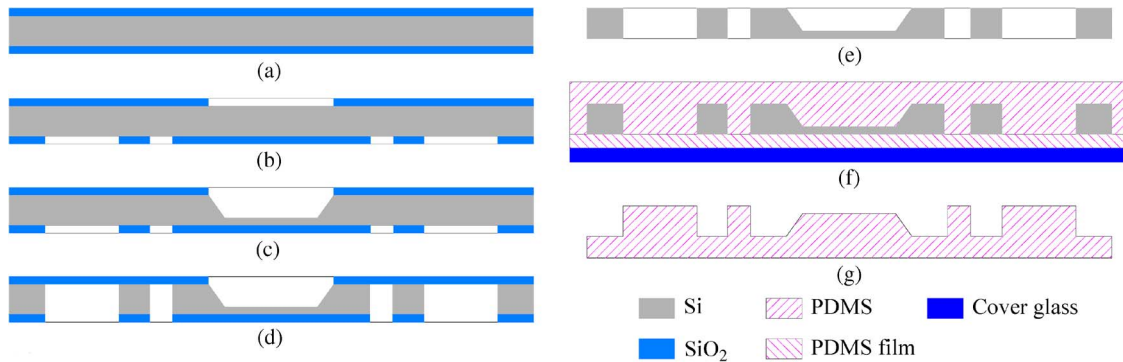


Fig. 7. Fabrication process of the dual-color TIR-based chip. (a) Oxidation. (b) Back- and front-side  $\text{SiO}_2$  patterning. (c) Front-side TMAH wet anisotropic etching. (d) Back-side DRIE. (e)  $\text{SiO}_2$  removal and smoothing lens by oxidation and BHF etching. (f) PDMS casting. (g) PDMS chip removal.

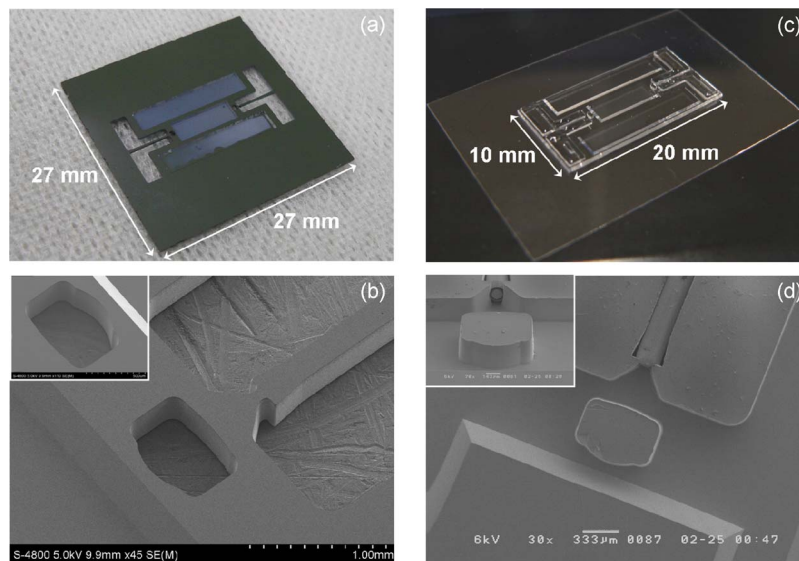


Fig. 8. (a) Photograph of the Si mold of the dual-color TIR-based chip. (b) SEM micrographs of one side of the Si mold. (c) Photograph of the PDMS chip (the dimensions of the chip are 20 mm  $\times$  10 mm  $\times$  0.9 mm in  $L \times W \times T$ ). (d) SEM micrographs of one side of the PDMS chip with glass capillary inserted.

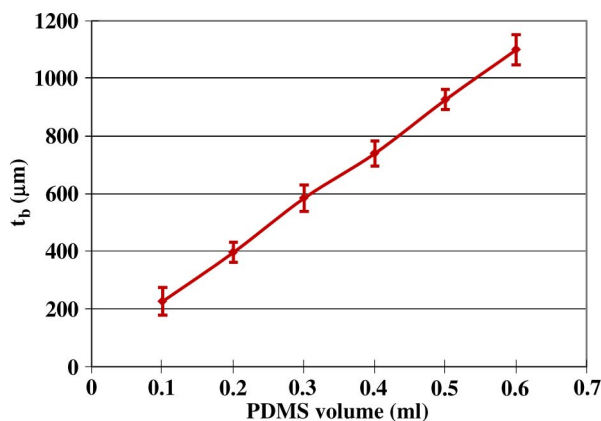


Fig. 9. Chip base thickness  $t_b$  versus PDMS volume during casting for the Si mold with a size of 27 mm  $\times$  27 mm.

all over the surface of the glass flow cell, only the dyes that were inside the evanescent fields were excited and emitted to form the TIR fluorescent spots. It is clearly seen that the TIR fluorescent spots from green and blue excitations have been separately generated when only one laser was turned on

[Fig. 11(a) and (b)] and overlapped when both lasers were turned on [Fig. 11(c) and (d)]. The green excitation was targeted to excite the TMR dye, while the blue excitation was targeted to excite the FI dye. However, due to its broad emission spectrum [Fig. 11(e)], fluorescence emission from FI can go through both ET 585/40 and ET 515/30 emission channels, as can be seen from Fig. 11(b). Although the lengths of the TIR fluorescent spots are beyond the field of view of a 10 $\times$  objective, the widths of the TIR fluorescent spots are measured to be approximately 90  $\mu\text{m}$  for both green and blue excitations [Fig. 11(a) and (b)]. There is a large discrepancy between the widths of the evanescent fields estimated by simulation (approximately 190  $\mu\text{m}$ ) as compared to the widths of the TIR fluorescent spots (approximately 90  $\mu\text{m}$ ) measured from the fluorescent images. This discrepancy could be due to the possibility that the single-mode fibers might have allowed transmission of more than one fundamental mode at 543 or 473 nm. At these wavelengths, the fundamental mode is much more confined to the core of the fiber and thus has a smaller MFD than the ideal MFD of 9.2  $\mu\text{m}$ , which was used in the simulation [38]. As can be seen in Fig. 11(a)–(d), there are a high-intensity region in the center excited by the fundamental mode and two much lower



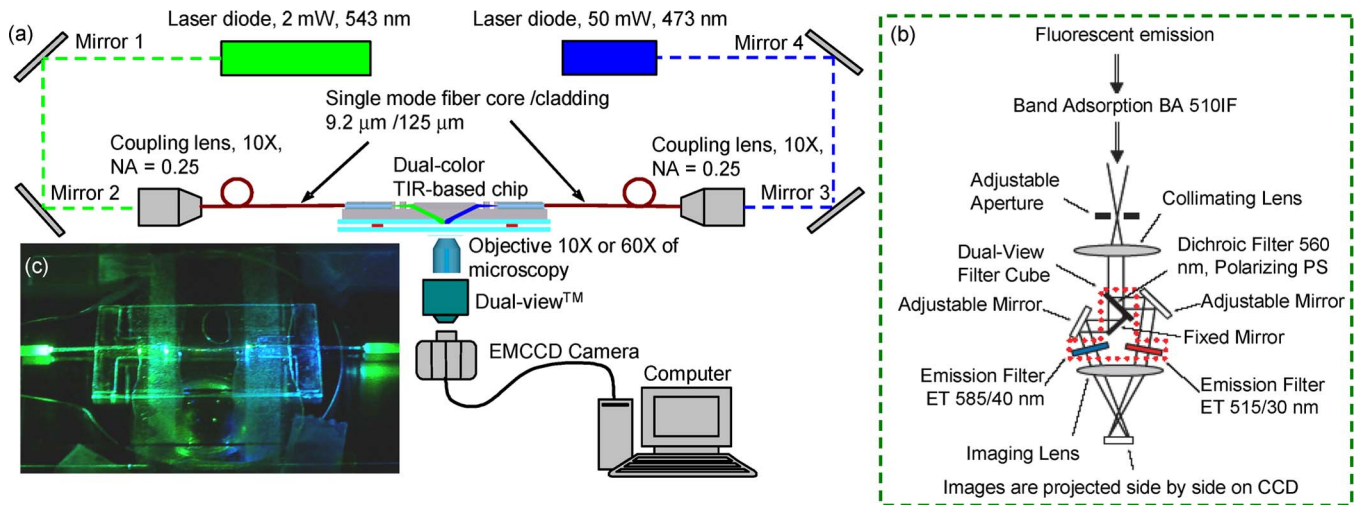


Fig. 10. (a) Experimental setup with Olympus IX71 inverted microscope with 10 $\times$  or 60 $\times$  objective, Dual-View, iXon EM+ DU-89 EMCCD camera, and two single-mode fibers (core/cladding = 9.2  $\mu$ m/125  $\mu$ m) coupling optics with Melles Griot laser diode (543 nm, 2 mW), Photop Suwtech laser diode (473 nm, 50 mW), four mirrors, and two coupling lenses. (b) Construction of Dual-View adapted from [http://www.magbiosystems.com/files/PDF/appnotes/dualview\\_appnote.pdf](http://www.magbiosystems.com/files/PDF/appnotes/dualview_appnote.pdf). (c) Close-up view of the chip setup on the stage of the microscope.

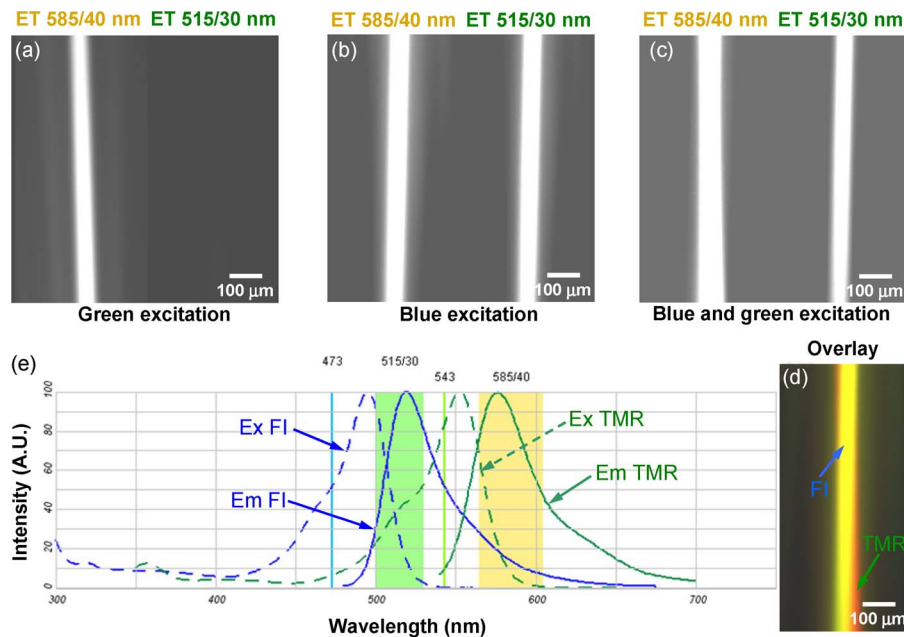


Fig. 11. Fluorescent images of the TIR fluorescent spots of a mixture of TMR dye (0.3 mM) and FI dye (3.3 mM) on the ET 585/40 and ET 515/30 emission channels when (a) only green excitation was turned on, (b) only blue excitation was turned on, and (c) both green and blue excitations were turned on are used. (d) Overlay pseudocolor image of ET 585/40 and ET 515/30 channels in (c). The fiber laser powers and exposure times in (a), (b), and (c) were all 0.52 mW and 300 ms, respectively. (e) (Dashed lines) Absorption and (solid lines) emission spectra of TMR and FI and their responses to emission filters and excitation laser sources, adapted from <http://probes.invitrogen.com>.

intensity regions on two sides of the high-intensity region that might be excited by the second mode. There have been several approaches to filter out the transmission of the higher modes in the single-mode fibers [31], [39], [40]. A small misalignment on the positions of the optical fibers along the longitudinal and vertical axes of the chip could also cause the variation on the size of the TIR fluorescent spots.

In previous work, the roughness transferred from the Si mold to the PDMS chip during the casting process has caused some fringe patterns of the TIR fluorescent spots [41]. In this paper, due to the smoothing of the Si lens mold fabricated by optimized DRIE and oxidation and BHF etching, we could achieve

uniform excitation by the fundamental mode, as observed in the TIR fluorescent spots. This uniformity is essential to ensure the uniform excitation of all fluorophores within the field of view. It is, however, necessary to eliminate the higher modes in the optical fibers so that the evanescent fields could be excited by only the fundamental mode.

### B. Imaging of Brownian Motion of Mixture of Suspensions of Fluorescent Microbeads

Fig. 12(a)–(c) shows the fluorescent snapshots of the Brownian motion of a mixture of suspensions of NR and DG

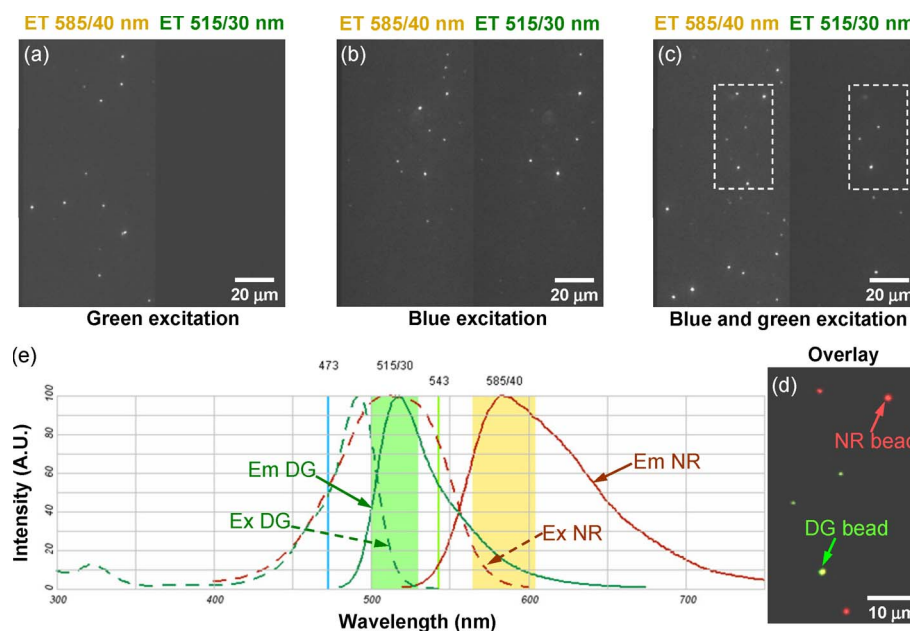


Fig. 12. Fluorescent snapshots of a mixture of suspensions of NR 0.5- $\mu\text{m}$  beads (0.05% *w/v*) and DG 0.5- $\mu\text{m}$  beads (0.05% *w/v*) suspended in Tween20/DI water solution on the ET 585/40 and ET 515/30 emission channels when (a) only green excitation was turned on, (b) only blue excitation was turned on, and (c) both green and blue excitations were turned on are used. (d) Overlay pseudocolor image of two regions of the ET 585/40 and ET 515/30 channels indicated in (c). The fiber laser powers and exposure times in (a), (b), and (c) were all 0.52 mW and 150 ms, respectively. (e) (Dashed lines) Absorption and (solid lines) emission spectra of NR and DG and their responses to emission filters and excitation laser sources, adapted from <http://probes.invitrogen.com>.

microbeads captured using the dual-color TIR-based chip on the ET 585/40 and ET 515/30 emission channels when the green laser was turned on, the blue laser was turned on, and when both lasers were turned on, respectively. The overlay of the highlighted regions from the two channels of Fig. 12(c) is shown in Fig. 12(d) with pseudocolors. Similar to imaging of fluorescent dyes, green and blue excitations were primarily aimed to excite the NR and DG microbeads, respectively. The broad emission spectrum of DG [Fig. 12(e)] also caused its fluorescence emission to go through both ET 515/30 and ET 585/40 channels, as seen in Fig. 12(b). Nevertheless, the evanescent-field illumination has significantly reduced the background noise that is commonly observed in epi-illumination mode [10]. This characteristic allows us to easily visualize individual NR and DG microbeads simultaneously as they randomly move vertically in and out of the overlapping evanescent fields. This high signal-to-noise level has enabled the single-color TIR-based devices to measure the microbead velocity and to detect single molecules of DNA [25].

## VI. CONCLUSION

A novel dual-color TIR-based chip for highly sensitive and high-resolution dual-fluorescence imaging has been presented. Optical analysis and simulation to confirm the overlap of two evanescent fields have been conducted. One could rely on the derived governing equations and vary the parameters to design the chips with different configurations. A low-cost simple fabrication method has been developed to integrate all miniaturized optical components into a monolithic PDMS chip. The monolithic PDMS chip can easily be integrated with various sample delivery platforms commonly used in  $\mu$ -TAS, namely glass slides, flow cells, microchannels, etc. The capability of the

chip for simultaneous dual-fluorescence imaging of two types of fluorescent dyes and two types of fluorescent microbeads has been experimentally demonstrated. The smooth PDMS lens has contributed to the uniform illumination of the evanescent fields, which is essential for the uniform excitation of all fluorophores in the field of view. Our device could be an alternative to conventional dual-color TIRFM. It could also potentially serve as a dual-color evanescent-excitation-based platform integrated into  $\mu$ -TAS for dual-fluorescence imaging.

## REFERENCES

- [1] D. Axelrod, T. P. Burghardt, and N. L. Thompson, "Total internal reflection fluorescence (in biophysics)," *Annu. Rev. Biophys. Bioeng.*, vol. 13, pp. 247–268, 1984.
- [2] X. H. N. Xu and E. S. Yeung, "Long-range electrostatic trapping of single-protein molecules at a liquid-solid interface," *Science*, vol. 281, no. 5383, pp. 1650–1653, Sep. 1998.
- [3] Y. Harada, T. Funatsu, K. Murakami, Y. Nonoyama, A. Ishihama, and T. Yanagida, "Single-molecule imaging of RNA polymerase–DNA interactions in real time," *Biophys. J.*, vol. 76, no. 2, pp. 709–715, Feb. 1999.
- [4] G. Seisenberger, M. U. Ried, T. Endreß, H. Büning, M. Hallek, and C. Bräuchle, "Real-time single-molecule imaging of the infection pathway of an adeno-associated virus," *Science*, vol. 294, no. 5548, pp. 1929–1932, Nov. 2001.
- [5] S. H. Kang, M. R. Shortreed, and E. S. Yeung, "Real-time dynamics of single-DNA molecules undergoing adsorption and desorption at liquid–solid interfaces," *Anal. Chem.*, vol. 73, no. 6, pp. 1091–1099, Mar. 2001.
- [6] Y. Sako and T. Yanagida, "Single-molecule visualization in cell biology," *Nat. Rev. Mol. Cell Bio.*, pp. SS1–SS5, Sep. 2003, Suppl. to vol. 4.
- [7] A. Yildiz, M. Tomishige, R. D. Vale, and P. R. Selvin, "Kinesin walks hand-over-hand," *Science*, vol. 303, no. 5658, pp. 676–678, Jan. 2004.
- [8] A. Yildiz, H. Park, D. Safer, Z. Yang, L. Q. Chen, P. R. Selvin, and H. L. Sweeney, "Myosin VI steps via a hand-over-hand mechanism with its lever arm undergoing fluctuations when attached to actin," *J. Biol. Chem.*, vol. 279, no. 36, pp. 37 223–37 226, Sep. 2004.
- [9] C. M. Zettner and M. Yoda, "Particle velocity field measurements in a near-wall flow using evanescent wave illumination," *Exp. Fluids*, vol. 34, no. 1, pp. 115–121, Jan. 2003.

- [10] S. Jin, P. Huang, J. Park, J. Y. Yoo, and K. S. Breuer, "Near-surface velocimetry using evanescent wave illumination," *Exp. Fluids*, vol. 37, no. 6, pp. 825–833, Dec. 2004.
- [11] R. Sadr, M. Yoda, Z. Zheng, and A. T. Conlisk, "An experimental study of electro-osmotic flow in rectangular microchannels," *J. Fluid Mech.*, vol. 506, pp. 357–367, 2004.
- [12] H. Gai, Y. Li, Z. Silber-Li, Y. Ma, and B. Lin, "Simultaneous measurements of the flow velocities in a microchannel by wide/evanescent field illuminations with particle/single molecules," *Lab Chip*, vol. 5, no. 4, pp. 443–449, Apr. 2005.
- [13] R. Sadr, M. Yoda, P. Gnanaprakasam, and A. T. Conlisk, "Velocity measurement inside the diffuse electric double layer in electro-osmotic flow," *Appl. Phys. Lett.*, vol. 89, no. 4, pp. 044103-1–044103-3, Jul. 2006.
- [14] A. Tengholm, M. N. Teruel, and T. Meyer, "Single cell imaging of PI3K activity and glucose transporter insertion into the plasma membrane by dual color evanescent wave microscopy," *Sci. STKE*, vol. 2003, no. 169, p. PL4, Feb. 2003.
- [15] J. Schmoranz and S. M. Simon, "Role of microtubules in fusion of post-Golgi vesicles to the plasma membrane," *Mol. Biol. Cell*, vol. 14, no. 4, pp. 1558–1569, Apr. 2003.
- [16] K.-H. Ikuko, R. Ken, F. Takahiro, I. Ryota, M. Hideji, S. K. Rinshi, and A. Kusumi, "Fluorescence imaging for monitoring the colocalization of two single molecules in living cells," *Biophys. J.*, vol. 88, no. 3, pp. 2126–2136, Mar. 2005.
- [17] S. H. Kang, Y.-J. Kim, and E. S. Yeung, "Detection of single-molecule DNA hybridization by using dual-color total internal reflection fluorescence microscopy," *Anal. Bioanal. Chem.*, vol. 387, no. 8, pp. 2663–2671, Apr. 2007.
- [18] S. Lee, B. H. Chung, and S. H. Kang, "Dual-color prism-type TIRFM system for direct detection of single-biomolecules on nanoarray biochips," *Curr. Appl. Phys.*, vol. 8, no. 6, pp. 700–705, Oct. 2008.
- [19] M. Leutenegger, H. Blom, J. Widengren, C. Eggeling, M. Gosch, R. A. Leitgeb, and T. Lasser, "Dual-color total internal reflection fluorescence cross-correlation spectroscopy," *J. Biomed. Opt.*, vol. 11, no. 4, pp. 040502-1–040502-3, Jul./Aug. 2006.
- [20] H. P. Lehr, A. Brandenburg, and G. Sulz, "Modeling and experimental verification of the performance of TIRF-sensing systems for oligonucleotide microarrays based on bulk and integrated optical planar waveguides," *Sens. Actuators B, Chem.*, vol. 92, no. 3, pp. 303–314, Jul. 2003.
- [21] H. P. Lehr, M. Reimann, A. Brandenburg, G. Sulz, and H. Klapproth, "Real-time detection of nucleic acid interactions by total internal reflection fluorescence," *Anal. Chem.*, vol. 75, no. 10, pp. 2414–2420, May 2003.
- [22] N. Chronis and L. P. Lee, "Total internal reflection-based biochip utilizing a polymer-filled cavity with a micromirror sidewall," *Lab Chip*, vol. 4, no. 2, pp. 125–130, 2004.
- [23] S. H. Huang and F. G. Tseng, "Development of a monolithic total internal reflection-based biochip utilizing a microprism array for fluorescence sensing," *J. Micromech. Microeng.*, vol. 15, no. 12, pp. 2235–2242, Oct. 2005.
- [24] N. C. H. Le, D. V. Dao, R. Yokokawa, J. Wells, and S. Sugiyama, "Design, simulation and fabrication of a total internal reflection (TIR)-based chip for highly sensitive fluorescent imaging," *J. Micromech. Microeng.*, vol. 17, no. 6, pp. 1139–1146, May 2007.
- [25] N. C. H. Le, R. Yokokawa, D. V. Dao, T. D. Nguyen, J. C. Wells, and S. Sugiyama, "Versatile microfluidic total internal reflection (TIR)-based devices: Application to microbeads velocity measurement and single molecule detection with upright and inverted microscope," *Lab Chip*, vol. 9, no. 2, pp. 244–250, Jan. 2009.
- [26] J. C. McDonald, D. V. Duffy, J. R. Anderson, D. T. Chiu, H. Wu, O. J. A. Schueller, and G. M. Whitesides, "Fabrication of microfluidic systems in poly(dimethylsiloxane)," *Electrophoresis*, vol. 21, no. 1, pp. 27–40, Jan. 2000.
- [27] D. A. Chang-Yen, R. K. Eich, and B. K. Gale, "A monolithic PDMS waveguide system fabricated using soft-lithography techniques," *J. Lightwave Technol.*, vol. 23, no. 6, pp. 2088–2093, Jun. 2005.
- [28] A. M. Cardenas-Valencia, J. Dlutowski, D. Fries, and L. Langebrake, "Spectrometric determination of the refractive index of optical wave guiding materials used in lab-on-a-chip applications," *Appl. Spectrosc.*, vol. 60, no. 3, pp. 322–329, Mar. 2006.
- [29] A. H. O. Karkkainen, J. T. Rantala, and M. R. Descour, "Fabrication of micro-optical structures by applying negative tone hybrid glass materials and greyscale lithography," *Electron. Lett.*, vol. 38, no. 1, pp. 23–24, Jan. 2002.
- [30] S. K. Das, "Modal noise due to short-wavelength (780–900-nm) transmission in single-mode fibers optimized for 1300 nm," *Appl. Opt.*, vol. 27, no. 3, pp. 552–556, Feb. 1988.
- [31] M. Stern, W. I. Way, V. Shah, M. B. Romeiser, W. C. Young, and J. W. Krupsky, "800-nm digital transmission in 1300-nm optimized single-mode fiber," in *Proc. Opt. Fiber Commun., OSA Tech. Dig. Series (Opt. Soc. Amer.)*, 1987, pp. MD2.
- [32] S. Franssila, J. Kiihamäki, and J. Karttunen, "Etching through silicon wafer in inductively coupled plasma," *Microsyst. Technol.*, vol. 6, no. 4, pp. 141–144, Apr. 2000.
- [33] W. T. Pike, W. J. Karl, S. Kumar, S. Vijendran, and T. Semple, "Analysis of sidewall quality in through-wafer deep reactive-ion etching," *Microelectron. Eng.*, vol. 73/74, no. 1, pp. 340–345, Jun. 2004.
- [34] C. H. Lee, K. Jiang, and G. J. Davies, "Sidewall roughness characterization and comparison between silicon and SU-8 microcomponents," *Mater. Charact.*, vol. 58, no. 7, pp. 603–609, Jul. 2007.
- [35] N. C. H. Le, D. V. Dao, R. Yokokawa, J. C. Wells, and S. Sugiyama, "Fabrication of optically smooth, through-wafer silicon molds for PDMS total internal reflection (TIR)-based devices," *Microsyst. Technol.*, published online, DOI: 10.1007/s00542-009-0913-3.
- [36] D. B. Kao, J. P. McVittie, W. D. Nix, and K. C. Saraswat, "Two-dimensional thermal oxidation of silicon—I. Experiments," *IEEE Trans. Electron Devices*, vol. ED-34, no. 5, pp. 1008–1017, May 1987.
- [37] S. Sinzinger and J. Jahns, *Microoptics*. Berlin, Germany: Wiley-VCH, 2003.
- [38] D. Marcuse, "Loss analysis of single-mode fiber splices," *Bell Syst. Tech. J.*, vol. 56, no. 5, pp. 703–718, May/Jun. 1977.
- [39] W. T. Anderson and T. A. Lenahan, "Length dependence of the effective cutoff wavelength in single-mode fibers," *J. Lightwave Technol.*, vol. 2, no. 3, pp. 238–242, Jun. 1984.
- [40] V. Shah, "Curvature dependence of the effective cutoff wavelength in single-mode fibers," *J. Lightwave Technol.*, vol. 5, no. 1, pp. 35–43, Jan. 1987.
- [41] N. C. H. Le, D. V. Dao, R. Yokokawa, J. Wells, and S. Sugiyama, "A dual-color total internal reflection (TIR)-based chip for simultaneous detection of two fluorophores," in *Proc. 7th IEEE Int. Conf. SENSORS*, Lecce, Italy, 2008, pp. 1191–1194.



**Nam Cao Hoai Le** received the B.Eng. degree in aeronautical engineering from Ho Chi Minh City University of Technology, Ho Chi Minh City, Vietnam, in 2003, the M.S. degree in advanced materials for micro- and nano-systems from the Singapore-MIT Alliance, National University of Singapore, Singapore, in 2004, and the Dr.Eng. degree in micro system technology from Ritsumeikan University, Shiga, Japan, in 2009.

From 2004 to 2005, he was with Nanoscience Innovation Pte. Ltd., Singapore, as a Research Engineer, developing advanced nanostructured materials and their applications. He is currently a Postdoctoral Researcher with the Biomedical Diagnostics Institute, Dublin City University, Dublin, Ireland. His current research interests are the design and fabrication of optical MEMS, optical biosensors, and microfluidics.



**Dzung Viet Dao** received the B.S. degree in informatics-mechanical engineering and the M.S. degree in machinery mechanics from Hanoi University of Technology (HUT), Hanoi, Vietnam, in 1995 and 1997, respectively, and the Ph.D. degree in science and engineering from Ritsumeikan University, Shiga, Japan, in 2003.

He became a Lecturer with the Faculty of Mechanical Engineering, HUT, in 1995. He was a Mechanical Engineer with Alcatel Telecom Company, Vietnam, from 1995 to 1999. In 1999, he joined Ritsumeikan University, where he was a Postdoctoral Fellow with the Micro Nano Integrated Devices Laboratory, Ritsumeikan University, from 2003 to 2005, was an Assistant Professor from 2005 to 2006, and is currently a Chair Professor with the Research Organization of Science and Engineering. His current interests are Si-based micromechanical sensors, microactuators, integrated MEMS, and polymer MEMS.





**Ryuji Yokokawa** (M'05) received the B.S. and M.S. degrees from the Kyoto University, Kyoto, Japan, in 2000 and 2002, respectively, and the Ph.D. degree from the University of Tokyo, Tokyo, Japan, in 2005. He also studied MEMS in the Mechanical and Aerospace Engineering Department, University of California, Los Angeles, from 2000 to 2001.

He was with the Department of Micro System Technology, Ritsumeikan University, Shiga, Japan, as an Assistant Professor from 2005 to 2009. He is currently an Assistant Professor in the Department of Microengineering, Kyoto University, Kyoto, Japan. He is also with Precursory Research for Embryonic Science and Technology (PRESTO), Japan Science and Technology Agency (JST), Saitama, Japan. His current research involves developing micro-total analysis systems by focusing on biomolecules, and integrating MEMS/NEMS and motor proteins for transport systems.



**John C. Wells** received the Doctorate degree in mechanics from the University of Grenoble I, Grenoble, France.

He has been with Ritsumeikan University, Shiga, Japan, as an Associate Professor in the Department of Civil and Environmental Engineering since 1999. His research interests are wall turbulence, particle image velocimetry and other flow-imaging techniques, and sediment transport micromechanics.



**Susumu Sugiyama** (M'94) received the B.S. degree in electrical engineering from Meijo University, Nagoya, Japan, in 1970, and the Dr.Eng. degree from Tokyo Institute of Technology, Tokyo, Japan, in 1994.

From 1965 to 1995, he was with the Toyota Central R&D Laboratories, Inc., where he worked on silicon sensors, integrated sensors, and micromachining. Since 1995, he has been with Ritsumeikan University, Shiga, Japan, where he was a Professor in the College of Science and Engineering, and is currently the Director of the Research Institute for Nanomachine System Technology and a Professor in the Ritsumeikan Global Innovation Research Organization. He is also a Guest Professor at Shanghai Jiao Tong University, Shanghai, China, and a Visiting Professor at Waseda University, Tokyo, Japan. In addition, he is the Editor-in-Chief of *Sensors and Materials*, the Executive Director of the Japan Institute of Electronics Packaging, and the President of the Sensors and Micromachines Society of the Institute of Electrical Engineers of Japan (IEEJ). His current interests are MEMS, integrated sensor systems, and synchrotron radiation 3-D lithography.

Dr. Sugiyama is a member of the IEEJ, the Japan Society of Applied Physics, the Robotics Society of Japan, and the Japan Society of Mechanical Engineers.